**SYNOPTIC: Two-Phase Plume Impingement Effects,** A. J. Laderman, C. H. Lewis, and S. R. Byron, Philco-Ford Corporation; *AIAA Journal*, Vol. 8, No. 10, pp. 1831–1839.

**Multiphase Flows: Hypervelocity Impact**

**Theme**

This paper presents the results of an experimental study to determine particle impingment forces and damage produced on flat plate models located at several angles of impingement in a controlled two-phase flow.

**Content**

Tests were conducted in a blow-down type, two-phase, supersonic wind tunnel using helium carrier gas to accelerate micron-sized aluminum oxide particles to velocities ranging from 1300 to 2300 m/sec. The particle mass flux ranged from 0.4 to 2.6 g/cm² sec which corresponds to conditions typical of the near field of solid-propellant motors. A number of target materials were tested including stainless steel, teflon, carbon cloth phenolic, quartz cloth phenolic, ATJ graphite, and pyrolytic boron nitride. In order to determine the effect of angle of incidence on the nature of the particle-surface interaction, the targets were designed to provide information on impingement forces over the full range from grazing to normal impact. Specifically, impact angles of 90° (normal), 60°, and 20° were selected. Force measurements were made with a three component balance. The balance was instrumented to detect directly the axial force and two bending moments, where the latter could be resolved into the transverse component of force and a pure residual moment acting on the target. In addition, the flowfield surrounding the target was examined photographically, using schlieren and light transmission and scattering techniques.

For the range of experimental conditions, the particle impact was found to be inelastic for moderate to large angles of incidence and partially elastic for grazing incidence. The measured forces, which were observed to be independent of particle size, shock layer gas density and target material, were less than the theoretical forces by an amount dependent only on the angle of incidence. The most significant experimental result, however, was the discovery that a dense debris layer, comprised primarily of spent projectile material, formed immediately ahead of the target, partially shielding it from subsequent impact by oncoming particles. Although a large fraction of the incident particle momentum diffused through the layer and was transferred to the target, a significant fraction of the incident particle kinetic energy was absorbed by the impact debris with a corresponding decrease in target damage. The latter effect was accentuated with increasing particle mass flux where relative target damage, i.e., the ratio of target mass loss to mass of impinging particles, was observed to rapidly diminish.

# Two-Phase Plume Impingement Effects

A. J. Laderman,* C. H. Lewis,† and S. R. Byron‡
*Philco-Ford Corporation, Newport Beach, Calif.*

**The results of an experimental study to determine particle impingement forces and damage produced on flat plate models located at several angles of impingement in a controlled two phase flow are reported. Tests were conducted with a two phase, supersonic wind tunnel using helium carrier gas and micron-sized aluminum oxide particles accelerated to velocities ranging from 1300 to 2300 m/sec. The particle mass flux incident on the target ranged from 0.4 to 2.6 g/cm² sec which corresponds to conditions typical of the near field of solid-propellant motors. Target materials included stainless steel and several typical ablators. The most significant experimental result was the discovery that, for this range of mass flux, a debris layer formed immediately ahead of the target, partially shielding it from subsequent impact by oncoming particles. The test results, which were similar for all target materials, showed further that the impact debris was comprised primarily of spent projectile material. While a large fraction of the incident particle momentum diffused through the layer and was transferred to the target, a significant fraction of the incident particle kinetic energy was absorbed by the impact debris with a corresponding decrease in target damage. The latter effect was accentuated with increasing particle flux where relative target damage, i.e., the ratio of target mass loss to mass of impinging particles, was observed to rapidly diminish.**

## Introduction

DURING high-altitude operation of solid-propellant rockets, the exhaust flow from the rocket nozzle undergoes a large expansion and the resulting two-phase plume occupies a large volume in space. As a consequence, nearby vehicles which pass through the plume may be subjected to forces and moments which can seriously alter their flight characteristics. Depending on the local properties of the plume, these forces may be due to the gas flow around the

Received July 16, 1969; revision received March 16, 1970. This work was supported by SAMSO, Air Force Systems Command, under Contract F04694-67-C-0051.

* Supervisor, Experimental Fluid Physics Section, Aeroneutronic Advanced Development Operation. Member AIAA.
† Senior Research Engineer, Fluid Mechanics Department, Aeroneutronic Advanced Development Operation. Member AIAA.
‡ Manager, Fluid Mechanics Department, Aeroneutronic Advanced Development Operation; now at Mathematical Sciences Northwest Inc., Seattle, Wash.

body, to particle impact on the surface of the body, or to contributions from both. In addition, particle impingement can result in a high heat transfer to the affected surface and may produce significant target damage.

The accurate determination of impingement effects requires a knowledge of the following: the mass and momentum flux distributions of the particle and gas streams throughout the undisturbed two phase plume; the resulting shock wave and subsequent interactions of the particle stream with the local environment ahead of the body; and the nature of the energy and momentum partition processes associated with the particle-surface interaction. This paper is concerned with the latter two aspects of the over-all problem and describes the results of experiments performed using flat plate models located at several angles of incidence in a controlled two phase flow. Force measurements were made using stainless steel and several ablative materials as targets and damage data, in terms of target mass loss, were also acquired from pre- and post-test weight measurements.

## Background

Relatively little attention has been directed so far toward evaluating the aerodynamic effect of rocket jet impingement on a body. Furthermore, these studies have been concerned primarily with gas-only plumes and with the exception of an experimental program reported by Rute[1] and a theoretical analysis presented by Adler et al.,[2] no information has appeared on the subject of forces induced by particle cloud impingement. Rute[1] employed a short duration solid-propellant rocket facility and measured impact forces on right circular cylinders located at various positions in the exhaust flow. Particle impingement forces were determined by subtracting the gas contribution, determined by integrating the measured pressure distribution, from the total force. However, because of the short duration, the complex model geometry, and the lack of detailed specification of the particle plume, no information on the nature of the particle-surface interaction could be deduced. For these same reasons, a direct comparison of Rute's results with those presented here could not be made.

In spite of the lack of information, it is possible under certain conditions to establish upper and lower bounds for the magnitude of the particle impact force. For example, when the gas density and the body size are sufficiently large, the particles achieve equilibrium with the gas flow before impinging on the body. As a result, the presence of the particles alters the gas pressure distribution over the body through changes introduced by the properties of the effective equilibrium mixture. For this case, the gas flowfield around the body can be calculated with existing techniques and the forces and moments determined accordingly. On the other hand, when the gas density and body size are small, the flow in the shock layer is uncoupled. When, in addition, the particle concentration is not too large, the particles impact on the body with negligible change in incident properties. In this limit, the particle impingement force can be calculated directly with a knowledge of the particle-surface interaction, e.g., elastic or inelastic collision. For the intermediate case, when coupling is sufficient to alter the properties of the incident particle stream, the particle induced force is then the result of both a change in the gas pressure distribution caused by the presence of the particles and to direct impact of the modified particle stream. In order to determine the incident stream properties, the gas-particle flowfield around the body must be calculated taking into account the particle lag.

When the particle collision is inelastic, the energy absorbed by the target may result in significant mass removal. While considerable data on target damage has been acquired in studies of hypervelocity impact phenomena, most of this work has been restricted primarily to single impaction of like on like materials, usually metals, involving projectile sizes of the order of a millimeter in diameter. In contrast, little effort has been devoted to the impingement of a cloud of $\mu$-sized particles. In particular, with one exception[3] there is no information available on the projectile-target combinations of interest here, i.e., alumina particles impacting on ablative targets. While the single impact studies indicate an inelastic impact for projectile velocities in the range typical for the particulate matter found in rocket exhaust plumes, the nature of the particle-surface interaction may be significantly different during impingement by a cloud of $\mu$-particles. It is instructive therefore to examine the gross features of the multiple impact process.

A typical particle concentration in the near field of a solid-propellant rocket exhaust is $10^5/cm^3$. Assuming a particle velocity of $10^5$ cm/sec, the particle flux is then $10^{10}$ particles/$cm^2$ sec. If we further assume a number mean particle radius of 1 $\mu$, the time interval between successive collisions at the same location on the target is about one msec. Walsh and Tillotson[4] have shown that the interaction time of a high-velocity impact varies directly as the radius of the crater formed by the impact. For projectiles on the 1 mm size range, the total interaction time, including mass ejection, is a few hundred $\mu$sec.[5] Since crater radius varies as the projectile radius, the total interaction time for the $\mu$ size particles typical of the rocket exhaust plume is considerably less than one $\mu$sec for each particle. Thus the time between successive impacts is extremely long compared to the interaction time, and each impact can be considered as an independent event.

There are, however, several important distinctions between single and multiple impactions. The first arises from the target heating produced during the impact process. For a particle cloud, target heating is a cumulative effect which raises the surface temperature of the material, resulting in a change in the strength of the target material and its mechanical behavior.

A second distinction arises from the scale of the process. Hooker et al.[6] examined specifically the effects of impingement by a cloud of $\mu$-sized particles and found that, except for grazing angles, the impact damage is nearly independent of angle. They pointed out that for a single impact, irregularities in the target surface are generally much smaller than the size of the projectile. For multiple impacts, however, the damage produced by the first few mono-layers of particles results in surface irregularities of the same scale as the particle. Consequently, the remaining particles impinge on a highly irregular surface and all subsequent impacts occur on an average at a near-normal incidence. Furthermore, the experiments of Denardo and Nysmith[7] and Moore et al.,[8] have indicated a significant strength scaling effect with crater size. This has been rationalized by several investigators[9,10] on the basis of the Griffith Theory of Failure[11] which suggests that the rupture strength of a material is inversely related to the size of the flaws or defects in the specimen. Thus, if the defect length along which failure occurs is assumed to be directly proportional to specimen size and if the penetration depth is taken as a representative dimension for the specimen, then the Griffith theory predicts an increase in effective target strength with decreasing particle size. This, in turn, implies a reduction in target damage for $\mu$-particle impaction.

A third difference between single and multiple impingement arises from the magnitude of the target mass loss. Klahr[12] has shown that a dense stationary dust cloud surrounding a space vehicle would be effective in reducing damage from micro-meteroids as a result of interparticle collisions which would occur within the cloud. Since single impact studies indicated that the ratio of target mass loss to projectile mass is in excess of unity, a similar possibility arises here inasmuch as the target ejecta could interfere with the incident particle cloud, thus changing the local environment and altering the particle-surface interaction. In particular, if the material eroded from the target moved at a relatively slow velocity, a blanket of debris could accumulate and shield the target from

subsequent impacts by the particle stream. This would not only reduce total target damage but could have also a significant effect on impingement forces. Since the results of recent tests of particle cloud impingment damage at Aeronutronic[13] indicated that target damage for the alumina projectile-aluminum target combination was several orders of magnitude less than that anticipated on the basis of single impact data, the occurrence of a debris blanket comprised of ejecta seemed highly unlikely. However in the course of the present program it was found that a dense debris layer, consisting primarily of spent projectile material rather than target ejecta, does form immediately adjacent to the exposed target surface and dominates the impingement process.

## Experimental Program

The measurements reported here were made in a blow-down type, two-phase, supersonic wind tunnel using helium carrier gas with micron-sized aluminum oxide particles. A number of target materials were tested including stainless steel (St St), teflon (TFE), carbon cloth phenolic (CCP), quartz cloth phenolic (QCP), ATJ graphite (ATJ), and pyrolytic boron nitride (PBN). In order to determine the effect of angle of incidence on the nature of the particle-surface interaction, the targets were designed to provide information on impingement forces over the full range from grazing to normal impact. Specifically, impact angles of 90° (normal), 60°, and 20° were selected. As an aid to data reduction, the projected area of the target, on a plane normal to the flow axis, was maintained constant and the target shape was restricted to a flat plate. Thus the targets were elliptical in shape becoming circular at normal incidence with a diameter (or minor axis) of 1.25 in.

The cold flow helium wind tunnel system is shown schematically in Fig. 1. Helium from the storage tanks (A) flowed through the pressure regulator (B) and passed through the pebble bed heater (D) where it was heated to the operating temperature. The pebble bed, which had sufficient capacity to maintain the helium outlet temperature within 30°K for a four second run, was heated initially by hot air which passed through a 5 kw electric heater (H) and then was vented to the atmosphere through an outlet in the top of the bed. The lines from the pebble bed to and including the subsonic part of the acceleration nozzle were insulated and heated to prevent stagnation temperature loss in the flowing gas. A portion of the helium flow from the pebble bed was bled from the main stream at (E) and was then bypassed to the particle feeder (F), where it was used to inject the $Al_2O_3$ particles into the remainder of the helium flow. A description of the particle feeder is presented in Ref. 14. The gas-particle mixture then passed into the wind tunnel (G), through the test section, and exhausted into a 3800 $ft^3$ vacuum tank (I). A burst diaphragm (C) was used to prevent over-pressurization of the system.

The axisymmetric wind-tunnel section of the cold flow facility was designed to produce a nominal Mach 8 gas-only flow in the test station. The initial sections of the tunnel

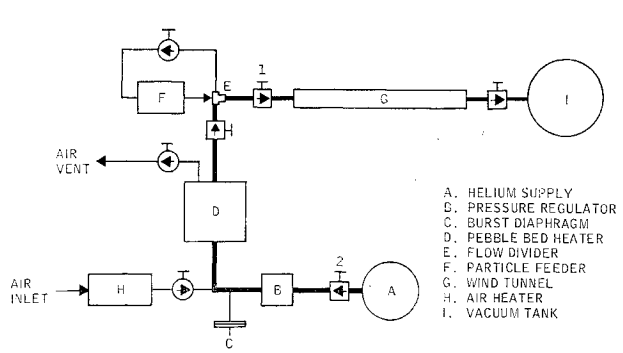


**Fig. 1 Schematic of cold flow facility.**

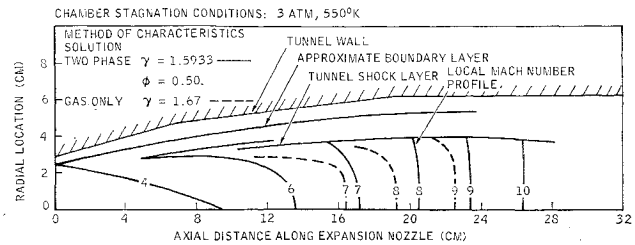


**Fig. 2 Helium tunnel test section flowfield.**

which comprise the acceleration nozzle serve the purpose of accelerating the $Al_2O_3$ particles to the required velocities (1300–2300 m/sec at 550°K). The acceleration section is 43 throat diam long and produces a Mach 4 flow at its exit. The gas-particle coupling in the supersonic portion of the nozzle is relatively high, resulting in efficient acceleration of particles as large as 10 $\mu$ in diam. For example at stagnation conditions of 3 atm and 550°K, a 10 $\mu$ particle is accelerated to over 1500 m/sec at $\phi = 0.5$ and to over 1700 m/sec at $\phi = 0.1$, where $\phi$, the particle loading, is the ratio of particle to gas mass flux.

The acceleration nozzle terminates in an effective diameter of 5 cm (the physical diameter is 5.9 cm to allow for the boundary layer) and is followed by a rapid expansion to the test section diam of 12.7 cm. The short expansion section provides a rapid reduction of the gas pressure down to the desired levels with minimum radial dispersion of the particle stream. In this manner, the particle momentum flux is made large compared to the gas pressure on the model, so that particle forces which are large compared to that of the gas pressure can be obtained for practical values of initial particle loading. The test section is shown schematically in Fig. 2, which includes also constant Mach number profiles for both a gas-only flow and a typical two-phase flow. The effective gamma which characterizes the latter case was determined using the method of Ref. 15.

Force measurements were made with a three component balance comprised essentially of a cantilever beam which attached to the target at its free end and to a rigidly mounted drag cage at its fixed end. The drag cage was instrumented to detect axial forces and the beam was instrumented at two locations to measure bending moments which could be resolved into the transverse component of force and pure residual moment acting on the target. Semiconductor strain gages, which provided adequate output over the entire range of operating conditions, were used in constant current bridge circuits to minimize nonlinear effects of the high sensitivity gages. The performance of the strain gauge circuits was monitored by repeated calibration during the test program. The procedure for data reduction to obtain the particle impact forces and moments, as well as other details on the experimental program, is described in detail in Ref. 14.

Two particle distributions were used in the program. A fine distribution, comprised of a commercially available metallurgical grade of $Al_2O_3$ manufactured by Linde Company and designated as Grade 1.0 C, ranged from 0.9 $\mu$ diam to 1.3 $\mu$ with a volume mean diam of about 1.0 $\mu$. Since no other commercially available distributions were available in the size range of interest from 5 to 10 $\mu$, a coarse, easily obtainable grade of $Al_2O_3$ was ground and classified in the laboratory to produce the second distribution extending from less than 1.0 to 15 $\mu$ and characterized by a number mean diam of 2 $\mu$ and a volume mean diam, $D_{30}$, of 5 $\mu$. Sizing was accomplished using a Sharples micromerograph. The ground particles were examined under a microscope and found to be irregularly shaped, although on the basis of random sampling the maximum length-to-breadth ratio was of the order of 1.5–2.0. In spite of the gross departure from a spherical shape it is of interest to note that the measured properties of the particle stream were in good agreement with those calcu-

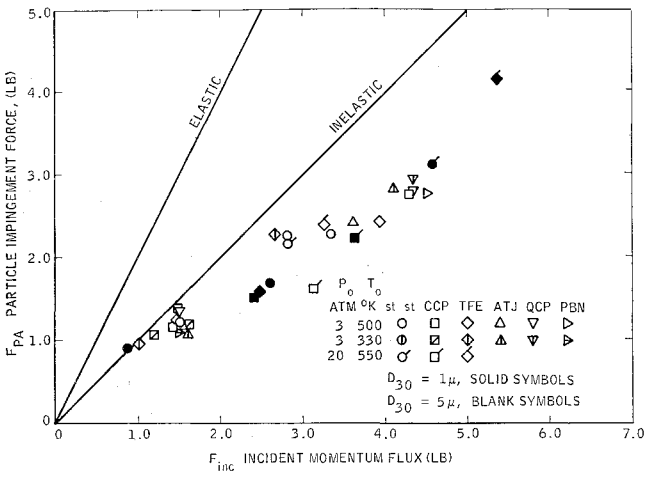


**Fig. 3 Particle impingement force for 90° targets.**

lated on the basis of the size characterization, in terms of equivalent diameter, provided by the micromerograph. The particles comprising the Linde sample were found to be of uniform size, approximately one $\mu$ in diam and within the resolution limit of the microscope (about 0.2 $\mu$) appear to be spherical in shape.

Prior to the performance of the test program documentation tests were performed to verify the design performance of the facility and to establish the validity of the two phase flow computations.[14] For most of the tests, the tunnel was operated at 3 atm and at stagnation temperatures of 500°K and 330°K. To examine the effect of gas-particle coupling, the tunnel was operated at stagnation conditions of 20 atm and 500°K. However, detailed calculations[14] indicated that, at these conditions, gas-particle coupling in the shock layer would be significant only for 90° impact with the 1.0 $\mu$ particles.

## Experimental Results

### Force Measurements

The axial component of the particle impingement force is plotted as a function of incident momentum flux in Figs. 3, 4A, and 5A for the 90°, 60°, and 20° models, while the transverse component for 60° and 20° targets is shown in Figs. 4B and 5B, respectively. Included also in the above figures are the theoretical curves for elastic and inelastic impact. The term "elastic" implies that the particle rebounds specularly from the surface of the target with its energy conserved, while in an "inelastic" collision the particle "sticks" or rebounds with zero velocity. The latter case assumes no target mass loss so that the resulting force represents the minimum for an inelastic impact. Therefore, for an elastic collision and the case of constant projected area

$$F_{PA} = F_{\text{inc}}[1 - \sin(90 - 2\theta)]$$

$$F_{PT} = F_{\text{inc}} \cos(90 - 2\theta)$$

where $F_P$ is the impingment force, $F_{\text{inc}}$ is the incident momentum flux, subscripts $A$ and $T$ denotes the axial and transverse components, respectively, and $\theta$ is the angle measured counterclockwise from the flow axis to the tangent to the surface, while, for the inelastic case

$$F_{PA} = F_{\text{inc}}$$

$$F_{PT} = 0$$

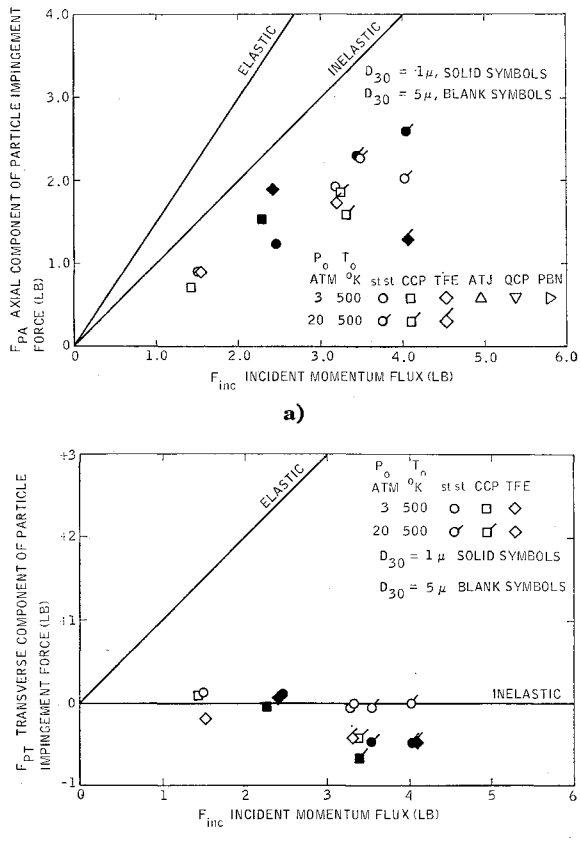


**Fig. 4 Particle impingement force for 60° targets; a) axial component, b) transverse component.**

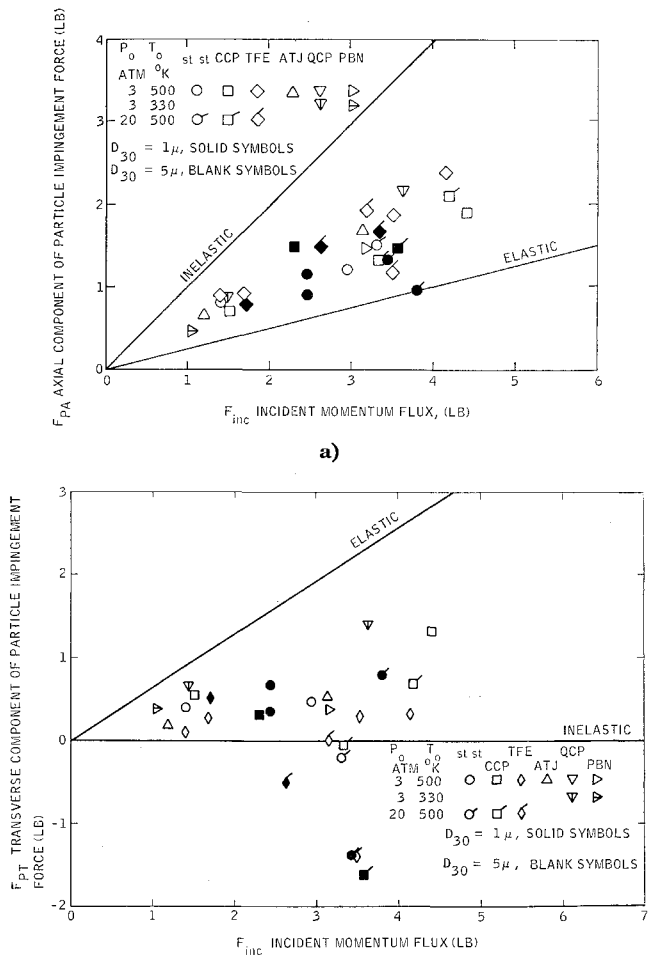


**Fig. 5 Particle impingement force for 20° targets; a) axial component, b) transverse component.**

From examination of the experimental results, several observations can be made. First, within the scatter of the experimental results, the measured impingement forces are independent of particle size, gas density, and target material. Secondly, it is possible, on the basis of the following discussion, to deduce, at least qualitatively, the nature of the particle-surface interaction.

For the conditions of the present experiments, the axial forces measured for 90° targets were found to be 20–25% less than the theoretical inelastic limit. A similar result was obtained for 60° targets, although the difference between theory and experiment was now approximately 40%. However, the measured transverse force component was found to be essentially zero, implying that the particle rebound momentum is negligible. Thus, for near normal incidence the particle impact can adequately be described as completely inelastic, although the discrepancy in the magnitude of the force indicates that the incident momentum is not completely transferred to the target and suggests that the particle stream is altered prior to impingement on the target. For 20° targets, the measured axial force component was again less than the theoretical inelastic limit but now greater than the elastic limit so that again this information alone was not sufficient to specify the particle-surface interaction. In this case, however, the transverse component was finite, but less than the elastic limit, indicating a partially elastic impact. Since, in addition, the transverse force measurements indicate greater momentum accommodation than the axial measurements, it is possible that for small angles of incidence the interaction process involves the same mechanism which produced the force deficit observed for the larger angles.

In summary then it appears that the particle impact is inelastic for moderate to large angles of incidence and partially elastic for grazing incidence and furthermore that the momentum of the incident particle stream is not completely transferred to the target. Additional insight to the impact process is derived from the interpretation of target damage data presented below.

### Target Damage Measurements

Although a considerable amount of data on target damage was obtained for both TFE and CCP, the former indicated a more consistent, reproducible trend with the significant experimental parameters. This has been attributed to differences in the physical structure of the two materials. TFE is a homogeneous substance with uniform properties, while CCP is a heterogeneous material which could exhibit appreciable variations in local properties. In addition, since fewer tests were performed with the remaining ablators, these data were not sufficient to yield a specific trend, although they were generally consistent with TFE results.

The data for TFE is shown in Fig. 6 where the relative target damage, i.e., the ratio of target mass loss to mass of impinging particles, is plotted against incident particle mass flux. Unlike the particle impact forces, the amount of target damage depends on the particle size, the angle of incidence, and the post-shock gas density (for convenience this parameter has been identified in terms of the tunnel stagnation conditions since the properties of the gas stream vary over the surface of the target). The target damage also depends on the material and, of the five ablators, TFE was found to be the most resistant to erosion while CCP experienced the greatest damage (approximately 2.5 times more than TFE at the lowest particle mass flux). The most significant aspect of Fig. 6, however, is the fact that relative target damage diminishes with increasing incident particle mass flux.

### Rationalization of Experimental Results

In addition to the quantitative damage measurements obtained during the cold flow tests, the targets exhibited a

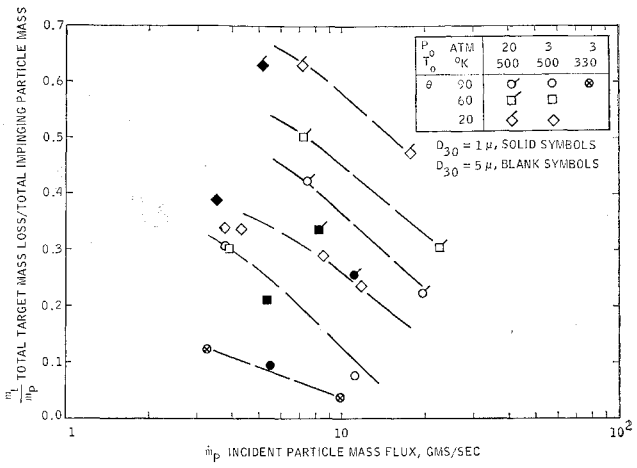


**Fig. 6 Relative damage for teflon targets.**

characteristic post-test configuration. For normal impact, the initially flat targets were found to be slightly rounded with minimum surface regression at the center, while for oblique impact the amount of surface regression decreased almost linearly with distance from the forward tip. The final shape of the target is a direct indication that the properties of the impinging particles vary continuously over the surface of the target. Since the flow documentation tests had clearly demonstrated the radial uniformity of the incident particle flow,[14] it is concluded that the particle stream is altered by interaction with the environment immediately surrounding the target. The two most obvious interaction mechanisms are gas-particle coupling and target shielding. Gas-particle coupling was found to be negligible at a stagnation pressure of 3 atm, while at 20 atm the flow was only moderately coupled for the 1 $\mu$ particles and essentially uncoupled for larger particles.[14] Consequently, particle coupling was eliminated as an effective mechanism in the present study and the observed results were attributed to target shielding. This, in fact, provides the most significant finding of the current work, i.e., there is a range of particle flux where debris from the particle impact partially shields the target from subsequent impingement thereby reducing both the induced force and the erosion rate.

## Discussion of Results

### Nature of Debris Layer

#### *Identification of debris material*

The experimental observations, in addition to establishing the existence of a debris layer, were also useful in specifying the source of the debris. First, as stated previously, the maximum ratio of mass of target removed to total mass of impinging particles was of the order of unity or less. Thus the mass addition from the target increased the total flux of particulate material around the target by at most a factor of two. Secondly, the force measurements for the stainless steel targets, which experienced negligible mass loss, exhibited the same behavior as those for the ablative materials. It seemed reasonable, therefore, that the steel targets would also be subjected to the same shielding effects observed for the ablators. These factors indicate that the impact debris is comprised primarily of spent projectile materials.

#### *Photographic studies*

In order to further demonstrate the existence of the debris layer, as well as to delineate its physical extent, several experiments were performed using photographic light scattering and transmission methods, and schlieren observations. The light

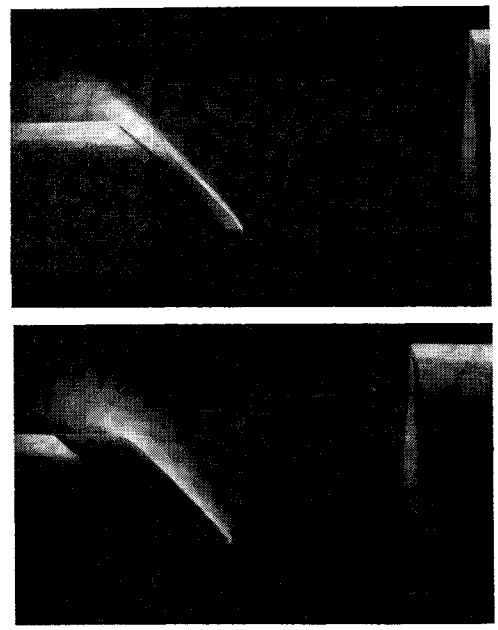


**Fig. 7 90° light scattering records of debris layer. Flow from right to left. a) CCP target, 45° b) TFE target, 45°.**

scattering experiments were carried out in a Mach 4 freejet facility which provides a flowfield similar to the closed wall test section used for the force measurements. This facility was equipped, just beyond the end of the nozzle, with four observation ports positioned 90° apart so that the target could be illuminated from above using a General Electric BH-6 mercury arc lamp, collimated to produce a narrow sheet of light parallel to the flow axis. Permanent records of the 90° scattered light were obtained photographically. Typical photographs for TFE and CCP targets inclined at 45° to the direction of particle flow are shown in Fig. 7. The shock layer density corresponds to that of the 20 atm tests in the Mach 8 wind tunnel. The nozzle exit plane is visible on the right hand side and the incident particle stream is well defined against a dark background by a low intensity of scattered light. The debris layer immediately adjacent to the exposed surface of the target is clearly obvious and the brightness of this zone contrasted to that of the incident stream gives a relative measure of the density of the layer.

Additional experiments, using light transmission and the Schlieren method, were performed in the cold flow wind tunnel. Light transmission records for 90° and 60° TFE targets are shown in Fig. 8. These photographs were obtained for a stagnation pressure of 3 atm and a particle mass flux incident on the target of 1.5 g/cm² sec. The target and holder appear now as shadows superposed on a bright background and the debris layer is recorded immediately ahead of the exposed target surface as a well defined dark zone whose general appearance is consistent with that observed in the light scattering experiments, Fig. 7. The light rays passing through the layer were completely attenuated indicating a large increase in particle concentration over its freestream value which is also in qualitative agreement with the light scattering results. A similar test for a 20° target, presented also in Fig. 8, showed no detectable attenuation of the light beam immediately ahead of the target. However the results of the force and damage measurements imply that the debris layer is less dense and that the particles rebound with greater velocity for 20° targets than for the other models. It is possible, therefore, that the change in particle concentration is too small to be detected by photographic means.

Simultaneous schlieren and light transmission observations were obtained using a 16 mm camera, operated at 64 frames/sec, to photograph the entire run. Typical frames selected from the gas-only and two phase portions of the test, which was performed under the same conditions as those for Fig. 8 are shown in Fig. 9. Note that in contrast to the initially flat surface of the target, the leading edge of the debris layer is slightly curved. The gas shock is well defined in both frames, although the photographic resolution is degraded slightly during the two-phase flow as a result of light scattered by the particles and of particles which deposit on the observation windows.

### *Model of debris layer*

For an inelastic impact, the particles, or fragments thereof, rebound from the surface with negligible velocity and, therefore, tend to accumulate in large concentration immediately ahead of the target. The photographs reveal that the debris layer is surprisingly thin and that its physical thickness, although varying slightly with target material, is a small fraction of the characteristic body dimension and less than the thickness of the shock layer. Furthermore, Fig. 7 and 8 indicate, through similarities in the appearance of the debris layer, that the regime of inelastic impact extends to angles of incidence as small as 45°. For grazing impact, in which case the interaction is partially elastic, the particles reflect from the target with appreciable rebound velocity. As a result the concentration of material within the debris layer is reduced. This has been confirmed by the light transmission records of Fig. 8 which show no detectable change in light intensity for 20° models compared to almost complete attenuation of the light beam at larger angles.

It is also clear that gas-particle coupling plays a significant role in the shielding mechanism although it is the coupling between the gas flow and the debris particles, rather than the incident particles, that is important. Although the drag force introduced by coupling has a negligible effect on the high

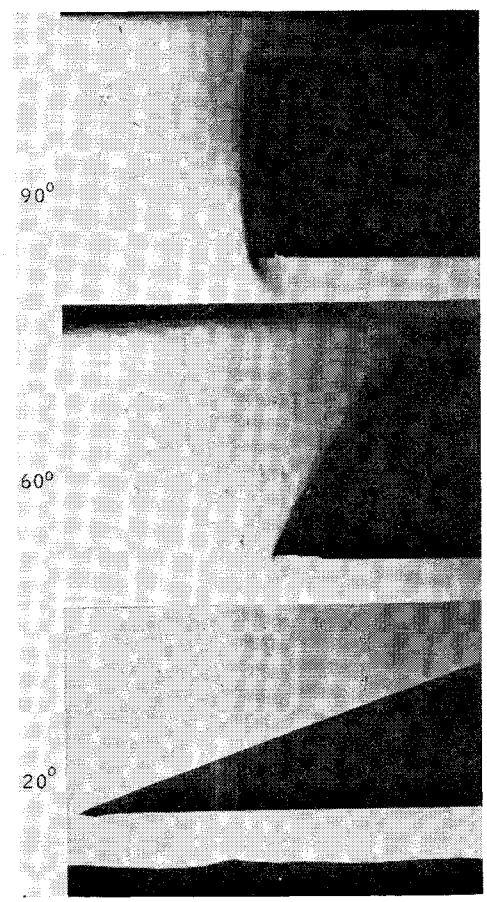


**Fig. 8 Light transmission records of debris layer. Flow from left to right. Stagnation conditions in the Helium tunnel; 3 atm, 300°K, $\phi$ = 0.30.**

speed incident particles, it has a relatively large influence on the subsequent trajectory of the initially low-speed debris. The photographic records show clearly that debris material is convected parallel to the surface of the target in the direction of gas flow. It is of interest to note further that at the edges of the target, where the gas expands rapidly and the flow is abruptly turned, the particle trajectories are relatively unaffected, indicating that the particles have decoupled from the low-density gas flow at the corners.

Since increased gas density enhances gas-particle coupling, it serves to augment the removal of debris material by convection. Consequently the shielding effectiveness of the impact debris should be reduced at higher gas density in the shock layer. This is indicated clearly in the TFE data of Fig. 10 where target damage has been replotted against the parameter $K\dot{E}\sin\theta$, which represents the particle kinetic energy flux per unit target surface area. Here the data separates into a family of curves according to the shock layer gas density (identified in terms of stagnation conditions) and is independent of particle size and angle of incidence.

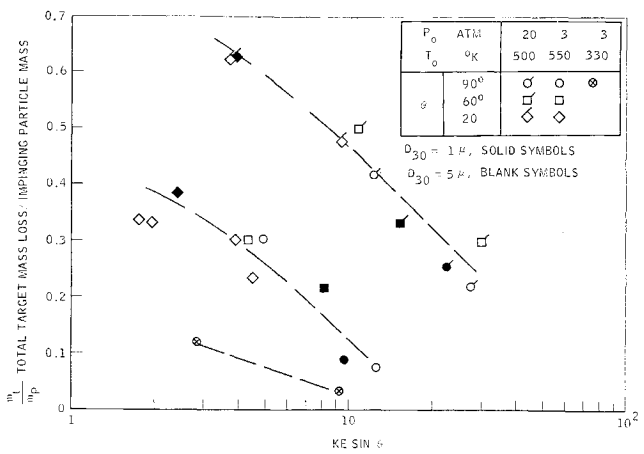


**Fig. 10 Correlation of Teflon target damage data showing effect of shock layer gas density.**

### Effect of Target Shielding

#### *Effect on momentum and energy accommodation*

On the basis of the foregoing discussion an important aspect of target shielding becomes clear. Although the debris layer was found to influence the accommodation of both the particle momentum and energy to the target surface, the effect on each process was significantly different. Specifically, the impingement force was observed to increase linearly with increasing particle mass flux, while the relative target damage diminished. In addition, the measured force was apparently independent of gas-particle coupling in the shock layer, while target damage increased with increasing post-shock gas density. Thus, regardless of the "thickness" of the debris layer, a large fraction of the incident particle momentum diffuses through it and is transferred to the target while the energy does not. This behavior may be attributed to the inter-particle collisions within the debris layer.

At low particle mass flux, when the layer is "thin," most of the incident particles reach the target without interference. However, as the mass flux increases, the layer becomes "thicker" and collisions between incident and reflected particles become more frequent. Eventually, the fraction of incident particles reaching the surface vanishes and the particles which do strike the target have experienced one or more collisions within the debris layer. The multiple collisions are effective in reducing the average velocity of the scattered particles which impact on the surface. Since the momentum of the particle stream is conserved, the reduced velocity is compensated for by an increase in the number of impinging particles and (with the exception of scattered particles which miss the target) the impact force is essentially unaltered by the presence of the debris layer.

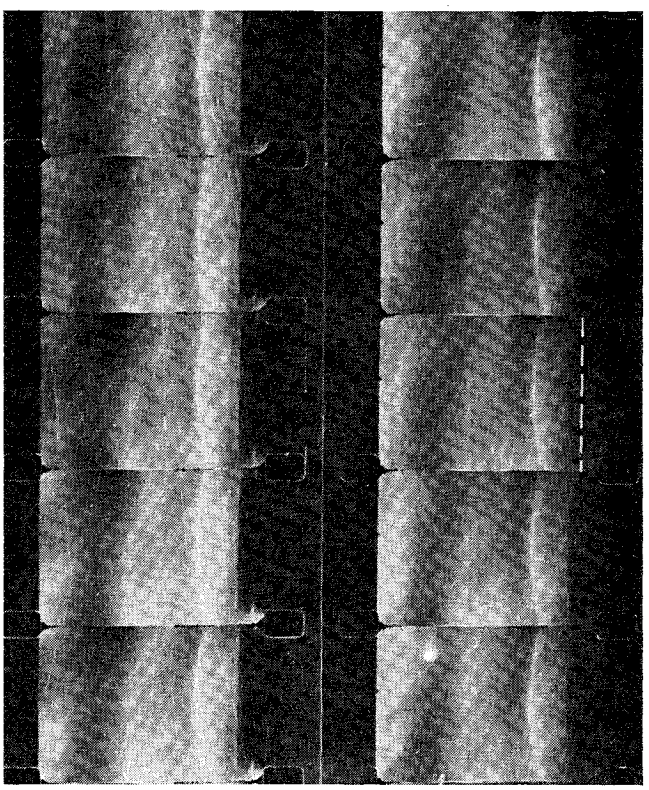

**Fig. 9 Simultaneous schlieren and light transmission observation of 90° TFE target during gas only (left) and two phase flow (right). Stagnation conditions: 3 atm, 300°K, $\phi = 0.30$. Flow is from left to right and target is located at right-hand-side of frame. Bright curved line ahead of target represents shock wave. White dashed line in center frame of two phase flow run indicates original surface of target.**

#### *Effect on partition of incident particle energy*

If the inter-particle collisions within the debris layer reduce the impact velocity as reasoned above, then the energy flux incident on the target is also reduced. Because the energy of the particle stream must also be conserved, the debris layer must act as a sink which absorbs the excess kinetic energy of the free stream particles. Since the debris material moves with a relatively small drift velocity, its kinetic energy must be small compared to its thermal energy. This has been substantiated qualitatively by visual observations of the target during the two-phase flow, when a zone of intense white-yellow luminosity was observed immediately ahead of the target. Further evidence that the debris layer reduces the energy flux to the target is provided by the results obtained from a similar study using aluminum targets.[16] In this program the partition of energy between the target and debris layer was determined on the basis of the measured target temperature and it was shown that the debris layer absorbs up to 90% of the incident kinetic energy flux.

#### *Effect on particle impingement heating*

In view of the experimental results, it is of interest to examine the effect of the debris layer on target heating produced by particle cloud impingement. Since the mechanism of energy partition between the debris layer and the target is still unknown, an exact analysis is not possible. However, based on the available data and with the introduction of suitable assumptions it is possible to estimate upper bounds to the

**Table 1 Estimates of steady-state target surface temperature**

| Material | $\dot{m}_p/A$, g/cm² sec | $q_0$, cal/cm² sec | Density, $\rho$ g/cm² | Specific heat, $c$ cal/g°C | Regression rate, $\dot{r}$ cm/sec | Approximate ablation temp. °C | Target temp. Eq. (4a) °C | Target temp. Eq. (4b) °C |
|---|---|---|---|---|---|---|---|---|
| TFE | 0.50 | 150 | 2.2 | 0.25 | 0.065 | 800 | [c] | 740 |
| TFE | 1.40 | 360 | 2.2 | 0.25 | 0.05 | 800 | [c] | 660 |
| CCP | 0.45 | 150 | 1.5 | 0.25 | 0.33 | 2800[b] | 600 | 360 |
| QCP | 1.55 | 360 | 2.6 | 0.30 | 0.32 | 2200[b] | 720 | 325 |
| ATJ | 1.30 | 360 | 1.7 | [a] | 0.18 | 2800 | 1500 | 640 |
| PBN | 1.65 | 360 | 2.2 | 0.45 | 0.25 | 2500 | 720 | 280 |

[a] Average specific heat, $c = 0.25$ for $T < 1200$°C, 0.4 for $T < 2000$°C.
[b] Binder decomposes at 800°C.
[c] Ablation temperature exceeded.

steady-state surface temperature of the target.§ Two cases are considered. In case 1, it is assumed that the oncoming particles pass through the debris layer unaffected, collide inelastically with the target and transfer to it their kinetic energy, and rebound without change in their thermal energy. This case, which leads to the maximum possible target temperature, ignores the presence of the debris layer and assumes that all of the freestream particle kinetic energy flux is absorbed by the target which loses mass at a constant rate. In case 2, the presence of the debris layer is accounted for by assuming that layer is in thermal equilibrium with the surface of the target. On the basis of the discussion presented in the previous section it seems reasonable that in the regime of strong shielding, such as that encountered in the present experiments, the debris layer receives energy directly from collisions with the oncoming particle stream as well as from the target and reflected particles. Consequently, it is unlikely that the layer is colder than the target and the assumption of thermal equilibrium provides a realistic upper limit to target temperature in the presence of debris shielding. A comparison of these two cases provides then an estimate of the reduction in target temperature resulting from the interaction between the particle stream and the debris layer.

With the exception of QCP, in which case the quartz melts at 2500°K, each of the ablative materials used in this program is a pure sublimer which sublimates at temperatures in excess of 2500°K. For both QCP and CCP, the phenolic binder decomposes at around 800°C, well below the ablation temperature for these materials. In a time of one second, which is the average duration of particle impingement, the depth of penetration of a thermal wave varies from a minimum of 0.03 cm for TFE to a maximum of 0.2 cm for ATJ and is, therefore, less than the minimum initial thickness (0.25 cm) of the targets. As a consequence, a simple model of one-dimensional heat transfer in a semi-infinite medium may be postulated.¶ Using a coordinate system where the exposed surface is fixed at the origin ($x = 0$) and the slab moves to the left at a uniform velocity equivalent to the average regression rate, $\dot{r}$, the steady-state heat conduction equation can be written as

$$\beta T_{xx} + \dot{r}T_x = 0 \tag{1}$$

subject to the boundary conditions

$$T(x \to \infty) = T_i \tag{2}$$

and, for Case 1,

$$q_0 - \dot{r}\rho c(T - T_i) = -kT_x,\ x = 0 \tag{3a}$$

while, for case 2

$$q_0 - \dot{r}\rho c(T - T_i) - (\dot{m}_p C_p/A)(T - T_{ip}) = -kT_x,\ x = 0 \tag{3b}$$

where $q_0$ is the incident kinetic energy flux per unit area, $\dot{m}_p/A$ is the particle mass flux per unit area, $c$ and $C_p$ are the specific heats and $T_i$ and $T_{ip}$ are the initial temperature of the target and particles, respectively, and $\beta$, $\rho$, and $k$ are, respectively, the thermal diffusivity, the density, and the thermal conductivity of the target. Integrating Eq. (1) and setting $x = 0$ yields for case 1

$$T - T_i = q_0/2\dot{r}\rho c \tag{4a}$$

and, for case 2

$$T - T_i = q_0'/[2\dot{r}\rho c + (\dot{m}_p C_p/A)] \tag{4b}$$

where $q_0' = q_0 + (\dot{m}_p C_p/A)(T_{ip} - T_i)$.

Results obtained using Eqs. (4a) and (4b) are shown in Table 1 for a number of typical run conditions. For all runs the gas stagnation temperature was 530°K, in which case the freestream particle temperature was approximately 150°K, while the initial target temperature was 300°K. With the exception of TFE, the target surface temperatures computed using Eq. (4a) are well below the ablation temperature and in the case of CCP and QCP also below the decomposition point of the binder. Using Eq. (4b) the surface temperatures are reduced 40% or more, depending on the mass loss ratio, and even in the case of TFE the surface temperature is now slightly less than the ablation temperature. Since both Eqs. (4a) and (4b) predict temperatures considerably less than the ablation temperature for all targets except TFE, the contribution of ablation to the observed surface regression cannot be significant. Therefore, it is concluded that for these materials mechanical erosion of the exposed surface is the principal mechanism of target damage. For TFE, the mechanism of target damage was further investigated by computing the steady state ablation rate corresponding to the energy flux reaching the target in cases 1 and 2. Assuming that the surface temperature, $T$, is constant and equal to its ablation value for case 1 or to the value calculated from Eq. (4b) for case 2, an energy balance at the exposed surface can be written as

$$q_0 - (\dot{m}_p C_p/A)(T - T_{ip}) - \rho\dot{r}\Delta H_s = -kT_x \tag{5}$$

where $\Delta H_s$ ($\approx$2000 cal/g) is the heat of ablation of TFE. Solving Eq. (1) subject to the conditions $T(x = 0) = T$ and $T(x \to \infty) = T_i$ and substituting the result into Eq. (5) yields

$$\dot{r} = [q_0 - (\dot{m}_p C_p/A)(T - T_{ip})]/\{\rho[\Delta H_s + c(T - T_i)]\} \tag{6}$$

where the term $(\dot{m}_p C_p/A)(T - T_{ip})$ in both Eqs. (5) and (6) is omitted for case 1. The ablation rates calculated using Eq. (6) are shown in Table 2 where, for comparison, the average experimental regression rates are included. For case 1, the calculated $\dot{r}$ exceeds the observed value for $q_0 = 360$ cal/

§ A crude analysis indicates that the time required for the build-up of the debris layer is of the order of $10^{-3}$ sec which is considerably less than the average test time in the present experiments.

¶ Rough calculations show that radiation losses are negligible compared to the incident kinetic energy flux.

**Table 2 Calculated ablation rates for TFE**

| $q_0$, cal/cm² sec | $\dot{r}$, cm/sec | | |
|---|---|---|---|
| | Exp. regression rate | Calc. | |
| | | Case 1 | Case 2 |
| 150 | 0.065 | 0.030 | 0.01 |
| 360 | 0.05 | 0.075 | 0.009 |

cm² sec, but is only half as large as the experimental regression rate when $q_0 = 150$ cal/cm² sec. For case 2 the computed $\dot{r}$ is over five times less than the observed rate of regression for both heat inputs. The fact that the observed surface regression diminishes slightly when $q_0$ is more than doubled is a direct indication that the energy flux reaching the target is less than its freestream value and, therefore, that the assumptions of case 1 are not appropriate to the present experiments. Since a decrease in the heating rate leads to reduced ablation rates it appears that even for TFE erosion plays a major role in target damage.

## Conclusions

On the basis of the experimental measurements it was possible to deduce the nature of the particle-surface interaction for a range of particle flux typical of the near field of many solid propellant motors and to delineate major differences between single and particle cloud impaction phenomena. Specifically, the following conclusions could be made.

For the range of velocities from 1300–2300 m/sec and mass flux from 0.4 to 2.6 g/cm² sec the particle impact was found to be inelastic for moderate to large angles of incidence and partially elastic for grazing incidence. While the experimental results were independent of particle size, shock layer gas density and target material, the measured forces were less than the theoretical forces by an amount dependent on only the angle of impingement. In contrast, the relative target damage was found to decrease with increasing incident particle mass flux, and to increase with increasing shock layer density.

The most significant finding, however, was the existence of a dense debris layer, comprised primarily of spent projectile material, immediately ahead of the exposed target surface which shielded the target from subsequent impact by oncoming particles. From a consideration of the inter-particle collisions within the layer, and the use of the conservation principles it was possible to rationalize the experimental observations on the basis of the "shielding" effect of the impact debris. Stated simply, a large fraction of the incident particle momentum diffuses through the debris layer and is transferred to the target surface while the incident particle energy is absorbed by the layer with only a small fraction transferred to the surface.

## References


[1] Rute, L., "Experimental Measurements of Solid Propellant Rocket Exhaust Effects at High Altitudes—Part II, Impingement Pressures, Forces, and Heat Transfer Rates in High Altitude Metallized Solid Propellant Rocket Exhaust Plumes," TR AFRPL-TR-67-223, *Proceedings of the AFRPL Two Phase Flow Conference*, Vol. II, San Bernardino, Aug. 1967, pp. 611–645.

[2] Adler, B. K., Schwartz, P. M., and Korkan, K. D., "Forces and Moments on Cylinders and Cones in a Two Phase Plume," *Journal of the Astronautical Sciences*, Vol. XIV, Nov.–Dec. 1967, pp. 290–299.

[3] Unger, E. W., "Particle Impacts on the Melt Layer of an Ablating Body," *ARS Journal*, Vol. 30, No. 9, Sept. 1960, pp. 799–805.

[4] Walsh, J. M. and Tillotson, J. H., "Hydrodynamics of Hypervelocity Impact," *Proceedings of the Sixth Symposium on Hypervelocity Impact*, Cleveland, Ohio, May 1963.

[5] Kineke, J. H., *Proceedings of the Fifth Symposium on Hypervelocity Impact*, Denver, Colo., Nov. 1961.

[6] Hooker, W. J., Watson, R., and Morsell, A. L., "Measurements with Powdered Solids in Shock Tubes," *The Physics of Fluids*, Vol. 12, No. 5, Supplement I, May 1969, pp. I-169–I-172.

[7] Denardo, B. P. and Nysmith, C. R., "Momentum Transfer and Cratering Phenomena Associated with the Impact of Aluminum Spheres into Thick Aluminum Targets at Velocities to 24,000 ft/sec," Paper presented at AGARD Fluid Dynamic Panel Specialists Meeting, Marseille, France, April 1964.

[8] Moore, H. J., Gault, D. E., and Heitowit, E. D., "Change of Effective Target Strength with Increasing Size of Craters for Hypervelocity Impact Craters," *Proceedings of Seventh Hypervelocity Impact Symposium*, Orlando, Fla., Feb. 1965.

[9] Evans, I. and Pomeroy, C. D., "The Strength of Cubes of Coal in Uniaxial Compression," *Mechanical Properties of Non-Metallic Brittle Materials*, edited by W. A. Walton, Interscience, New York, 1959.

[10] Gault, D. E. and Moore, H. J., "Scaling Relationship for Microscale to Megascale Impact Craters," *Proceedings of Seventh Symposium on Hypervelocity Impact*, Orlando, Fla., Feb. 1965.

[11] Griffith, A. A., "The Theory of Rupture," *The Proceedings of the International Congress of Applied Mechanics*, Delft, The Netherlands, 1924, pp. 56–63.

[12] Klahr, C. N., "Dustwall Shielding Against Meteoroids," *Proceedings of Seventh Symposium on Hypervelocity Impact*, Orlando, Fla., Feb. 1965.

[13] Kuby, W. C. and Lewis, C. H., "Experimental Study of the Effects of Particle Cloud Impingement," *AIAA Journal*, Vol. 6, No. 7, July 1968, pp. 1385–87.

[14] Laderman, A. J., Lewis, C. H., and Byron, S. R., Final Report on "Two Phase Plume Impingement Forces," SAMSO Contract F04694-67-C-0051, Aug. 1968, Aeroneutronic Publication U4429, Aeroneutronic Div. of Philco-Ford Corp., Newport Beach, Calif.

[15] Hoglund, R. F., "Recent Advances in Gas-Particle Nozzle Flows," *ARS Journal*, Vol. 32, No. 5, May 1962, pp. 662–671.

[16] Lewis, C. H. and Laderman, A. J., "Effects of Debris Shielding on Energy Partition," *Journal of Spacecraft and Rockets*, Vol. 6, No. 12, Dec. 1969, pp. 1470–72.